PNAS RESEARCH ARTICLE | AGRICULTURAL SCIENCES OPEN ACCESS

D-amino acid aminotransferase1 regulates grain chalkiness in rice by modulating endoplasmic reticulum stress response

Hui Dong[a,1], Jie Lei[a,1], Yunlu Tian[a,1], Juan Liu[b,1], Hang Yang[a], Xiaokang Jiang[a], Rushuang Zhang[a], Yu Zhang[a], Rongbo Chen[a], Yiqun Bao[c], Feng Liu[c], Yulong Ren[d], Yaping Lu[c], Xi Liu[a], Shijia Liu[a], Xue Yang[a], Erchao Duan[a], Xuan Teng[a], Yunlong Wang[a], Chuanwei Gu[a], Yipeng Zhang[a], Xiaoli Chen[a], Yunpeng Zhang[a], Hongyi Xu[a], Rui Sha[a], Xia Xu[b], Ruomeng Li[b], Gongyu Li[b,2], Yihua Wang[a,2], and Jianmin Wan[a,d,2]

Affiliations are included on p. 11.

Edited by Yibo Li, Huazhong Agriculture University, Wuhan, China; received July 19, 2025; accepted January 27, 2026 by Editorial Board Member Qifa Zhang

D-amino acids are key components of the bacterial cell wall and play important roles in neural communication and inflammatory responses in animals. However, knowledge about D-amino acid metabolism and physiological functions in plants is limited. Here, we isolated and characterized a rice *D-amino acid aminotransferase1*, *OsDAAT1*, which maternally regulates rice grain chalkiness through map-based cloning and a subsequent complementation test. We found that *OsDAAT1* is highly expressed in the vascular tissue of rice nodes and is capable of interconverting different D-amino acids in vitro. Mutation of *OsDAAT1* results in elevated D-alanine levels in stems, nodes, and developing grains. The disruption of D-amino acid metabolism subsequently leads to significantly altered peptide/protein isomerization, including some key enzymes involved in starch and protein biosynthesis. These changes trigger severe endoplasmic reticulum stress and ultimately leads to chalky grains. Furthermore, we identified $OsDAAT1^{Hap1}$ as a low-chalkiness haplotype, and historical frequency analysis suggests that *OsDAAT1* may have undergone selection during rice domestication. Overall, our findings uncover a previously unrecognized role in D-amino acid metabolism in plants and facilitate the practical use of *OsDAAT1* in grain appearance quality improvement in rice.

rice | grain chalkiness | D-amino acid aminotransferase | endoplasmic reticulum stress | peptide/protein isomerization

Significance

Improving grain appearance is a priority for rice breeding, as chalkiness markedly reduces commercial value. Here, we identify a previously unrecognized metabolic pathway involving D-amino acids that regulates this trait. We show that the *D-amino acid aminotransferase1*, *OsDAAT1*, maternally regulates grain chalkiness mainly through modulating D-amino acids metabolism, leading to the altered peptide/protein isomerization and the induction of endoplasmic reticulum stress during seed development. Importantly, we identified specific nucleotide polymorphisms in the *OsDAAT1* promoter that underlies natural variation in chalkiness among rice germplasms. Our findings reveal a previously unappreciated layer of genetic control of grain appearance quality and uncovers the pivotal role of D-amino acids metabolism in seed development, offering strategies for molecular breeding.

Grain chalkiness is a major constraint on rice quality that reduces consumer preference, increases breakage during milling, and compromises eating quality. Defined by opaque regions within the endosperm, chalkiness is classified as white-base, white-belly, white-core, or milky-white types (1). Although studies of milky-white mutants have linked chalkiness to defects in storage biosynthesis and organelle function, most cultivars display white-base, white-belly, or white-core phenotypes. These forms of chalkiness represent complex quantitative traits governed by intricate genetic and environmental interactions (2). To date, only four major natural quantitative trait loci, *OsTPS8*, *Chalk5*, *WCR1*, and *OsbZIP60*, have been characterized (3–6). Thus, the molecular mechanisms underlying natural variation in chalkiness formation remain largely unknown.

L-amino acids are the building blocks of proteins across all kingdoms of life. Nineteen L-amino acids have corresponding D-enantiomers as free forms or peptide-bound D-amino acids, with the exception of glycine which lacks a chiral center (7). In bacteria, D-alanine (D-Ala) and D-glutamate (D-Glu) are basic components of the peptidoglycan cell wall (8, 9). In animals, various D-amino acids have been detected and studied. For example, D-serine (D-Ser) and D-aspartic acid (D-Asp) regulate neurophysiological functions by binding to the N-methyl-D-aspartate receptor, an ionotropic glutamate receptor at the excitatory synapses (10–12). Recent studies have established that D-amino acids are also ubiquitously present in plants, which can be absorbed from the rhizosphere or de novo synthesized (13–15). One major source of endogenous plant D-amino acids originates from the racemization of L-amino acids to their respective D-enantiomers, a reaction catalyzed by racemases, such as alanine, serine, and tryptophan racemases (16, 17). Furthermore, endogenous D-amino acids can be interconverted through the transamination activities of D-amino acid aminotransferases. For example, in *Arabidopsis thaliana*, the D-amino acid transaminase AtDAT1 is proposed to catalyze the conversion of D-Asp to D-Glu or D-Ala (18).

D-amino acids have been shown to play important roles in plant development and stress resistance. For instance, D-Ser in the pistil is required for pollen tube growth by regulating glutamate receptor AtGLR1.2 mediated Ca^{2+} channels in *Arabidopsis* (19, 20). D-Ala, a component of peptidoglycan, has been detected in the plastid envelope of the

This article is a PNAS Direct Submission. Y.L. is a guest editor invited by the Editorial Board.

[1]H.D., J. Lei, Y.T., and J. Liu contributed equally to this work.

[2]To whom correspondence may be addressed. Email: ligongyu@nankai.edu.cn, yihuawang@njau.edu.cn, or wanjm@njau.edu.cn.

This article contains supporting information online at https://www.pnas.org/lookup/suppl/doi:10.1073/pnas.2519395123/-/DCSupplemental.

Published March 6, 2026.

moss and acts as a stress signal, with its accumulation observed in duckweed seedlings under ultraviolet stress (21, 22). Moreover, D-Ala can be absorbed and assimilated as nitrogen source by wheat (15). However, exogenous application of D-amino acids at high, nonphysiological concentrations, is generally considered detrimental to plant growth and development (23). Thus, how D-amino acids function in plants is largely unknown.

In this study, we demonstrate that *OsDAAT1* encodes a D-amino acid aminotransferase in rice, that mediates the interconversion of various D-amino acids. Mutation of *OsDAAT1* leads to the most prominent accumulation of D-Ala and triggers constitutive endoplasmic reticulum (ER) stress response. Furthermore, our results indicate that altered D-amino acid levels caused the changed peptide/protein isomerization, potentially interfering with protein folding and processing during seed development, thereby contributing to the formation of chalky grains. Collectively, these results indicate that *OsDAAT1* plays an important role in regulating rice grain chalkiness by modulating D-amino acid metabolism. Moreover, natural variations in *OsDAAT1* promoter region are significantly associated with grain chalkiness, offering a potential target for rice quality improvement.

Results

Phenotypic Characterization and Map-Based Cloning of *OsDAAT1*. To gain deep insights into the molecular mechanisms governing grain chalkiness, we screened a tissue culture-derived population of the *japonica* rice cv Nipponbare for chalky grain mutants. One mutant, *daat1*, produced seeds with extremely high chalkiness in the belly region (Fig. 1*A*). Compared to the wild type (WT), the *daat1* mutant showed a significant increase in both the percentage of grains with chalkiness (PGWC) and the degree of endosperm chalkiness (DEC; Fig. 1 *B* and *C*). Moreover, the *daat1* mutant exhibited a slower grain-filling rate and reduced 1,000-grain weight (Fig. 1*D* and *SI Appendix*, Fig. S1*A*), accompanied by significant decreases in plant height, tiller number, panicle length, primary and secondary branch number, seed setting rate (*SI Appendix*, Table S1). Biochemical analyses of *daat1* grains revealed reduced levels of total starch, amylose, and protein, accompanied by disrupted storage reserve balance, specifically regarding starch-to-protein and protein-to-amylose ratios, as well as altered protein composition (*SI Appendix*, Fig. S1 *B–J*). Collectively, these results demonstrate that *OsDAAT1* has significant effects on rice growth and development apart from chalkiness formation.

The embryo and the endosperm of seeds originate from double fertilization and contain filial genetic information. When the maternal plant represents the parental generation, the embryo within the seed constitutes the next generation (24). In our study, reciprocal crosses using *daat1* and WT plants revealed that F_1 seeds developing on the *daat1* maternal plant exhibited chalky grain, whereas *daat1* used as the male parent produced F_1 seeds with a WT-like transparent phenotype (*SI Appendix*, Fig. S2 *A* and *C*). These results indicated that the chalkiness phenotype is determined by the maternal tissue environment. Then, both seeds from reciprocal F_1plants (*daat1*/WT and WT/*daat1*) displayed transparent grains, similar to WT phenotype (*SI Appendix*, Fig. S2 *B* and *C*). Furthermore, when we grew the F_2 population, the genotypes of the F_2 individual plants segregated according to the Mendelian ratio of WT: heterozygous: homozygous as 1:2:1. We counted the number of plants producing entirely chalky seeds vs. those producing transparent seeds, which fitted a 3:1 ratio (Transparent grain plants: Chalky grain plants) (*SI Appendix*, Table S2). Collectively, these findings demonstrate that the grain chalkiness phenotype in *daat1* is maternally controlled.

Using 46 recessive individuals from the *daat1*/N22 F_2 population, we initially mapped the *daat1* locus to the region between simple sequence repeat (SSR) markers RM282 and Q3 on Chr. 3. Subsequent fine mapping with 2,309 F_2 individuals exhibiting the chalky grain delimited the interval to a 48-kb region flanked by markers Q1 and Q28, which contains seven open reading frames (ORFs) (Fig. 1*E*). Sequencing analysis revealed a 4,931-bp deletion in this region, encompassing the entire *LOC_Os03g24470* locus and extending to the fourth exon of *LOC_Os03g24460*. This genomic deletion caused a 448-bp loss within the coding sequence (CDS) of *LOC_Os03g24460*, resulting in altered structure of encoded protein (Fig. 1 *E* and *F*). Since *LOC_Os03g24470* encodes a hypothetical protein with low expression, we prioritized *LOC_Os03g24460* as the candidate gene. The deletion was verified by PCR and nearly abolished *LOC_Os03g24460* expression (Fig. 1 *G* and *H*). To validate the candidate gene, we constructed genomic complementation (GC) transgenic line with the *daat1* mutant with the CDS of *LOC_Os03g24460* driven by its native promoter. All positive transgenic lines displayed significantly reduced PGWC and DEC compared to *daat1*, effectively rescuing the chalky phenotype (Fig. 1 *I–K*). Furthermore, CRISPR/Cas9-generated homozygous knockout lines of *LOC_Os03g24460* in Nipponbare phenocopied the *daat1* defects (*SI Appendix*, Fig. S3 *A–C*). Notably, *wsd1*, an allelic mutant of *daat1*, displays a similar chalky grain phenotype (*SI Appendix*, Fig. S3*D*) (25). Collectively, these results establish *LOC_Os03g24460* as the causative gene underlying the *daat1* phenotype.

To further verify the maternal control of grain chalkiness, we silenced *OsDAAT1* using either the constitutive *Ubiquitin* (*Ubipro*) or the endosperm-specific *GlutelinC* (*GluCpro*) promoter. Constitutive silencing (*Ubipro:RNAi-OsDAAT1*), which down-regulated *OsDAAT1* expression in vegetative tissues and endosperm, recapitulated the chalky grain phenotype as indicated by the elevated PGWC and DEC. In contrast, endosperm-specific silencing of *OsDAAT1* (*GluCpro:RNAi-OsDAAT1*) produced normal transparent seeds (Fig. 1 *I–L*). Coupled with our population analysis (*SI Appendix*, Fig. S2), the full transparent grain developed in endosperm-specific silencing lines indicates that *OsDAAT1* regulates grain chalkiness via maternal tissues rather than through its function within the endosperm.

***OsDAAT1* Encodes a Functional D-Amino Acid Aminotransferase in Rice.** Transcript profiling revealed that *OsDAAT1* is expressed primarily in vegetative tissues, particularly in the node (Fig. 2*A* and *SI Appendix*, Fig. S4*A*). In situ hybridization further localized *OsDAAT1* transcripts to the vascular tissues of the first node (Fig. 2*B*), an expression pattern consistent with a maternal role in seed development. Immunoblotting confirmed that the OsDAAT1 protein is abundant in nodes and endosperm, but less in leaves and stems (Fig. 2*C* and *SI Appendix*, Fig. S4*B*). Subcellular localization assays using both transient expression in protoplasts and stable *35Spro*::*OsDAAT1-GFP* complementation of the *daat1* mutant placed OsDAAT1 in the cytosol (Fig. 2 *D* and *E* and *SI Appendix*, Fig. S4 *C–F*). This result was corroborated by subcellular fractionation of developing endosperm, where OsDAAT1-GFP was detected exclusively in soluble fractions (S2, S13, and S100), mirroring the cytosolic marker OsAlaAT1 (26) (Fig. 2*E*). Collectively, these data establish OsDAAT1 as a cytosolic protein.

OsDAAT1 encodes a protein of 563 amino acids that harbors a conserved D-amino acid aminotransferase domain (Fig. 2*F*). Phylogenetic analysis showed that proteins homologous to OsDAAT1 are widely distributed across eukaryotes and prokaryotes (*SI Appendix*, Fig. S5). To investigate whether OsDAAT1 is capable of interconverting different D-amino acids, we first analyzed the

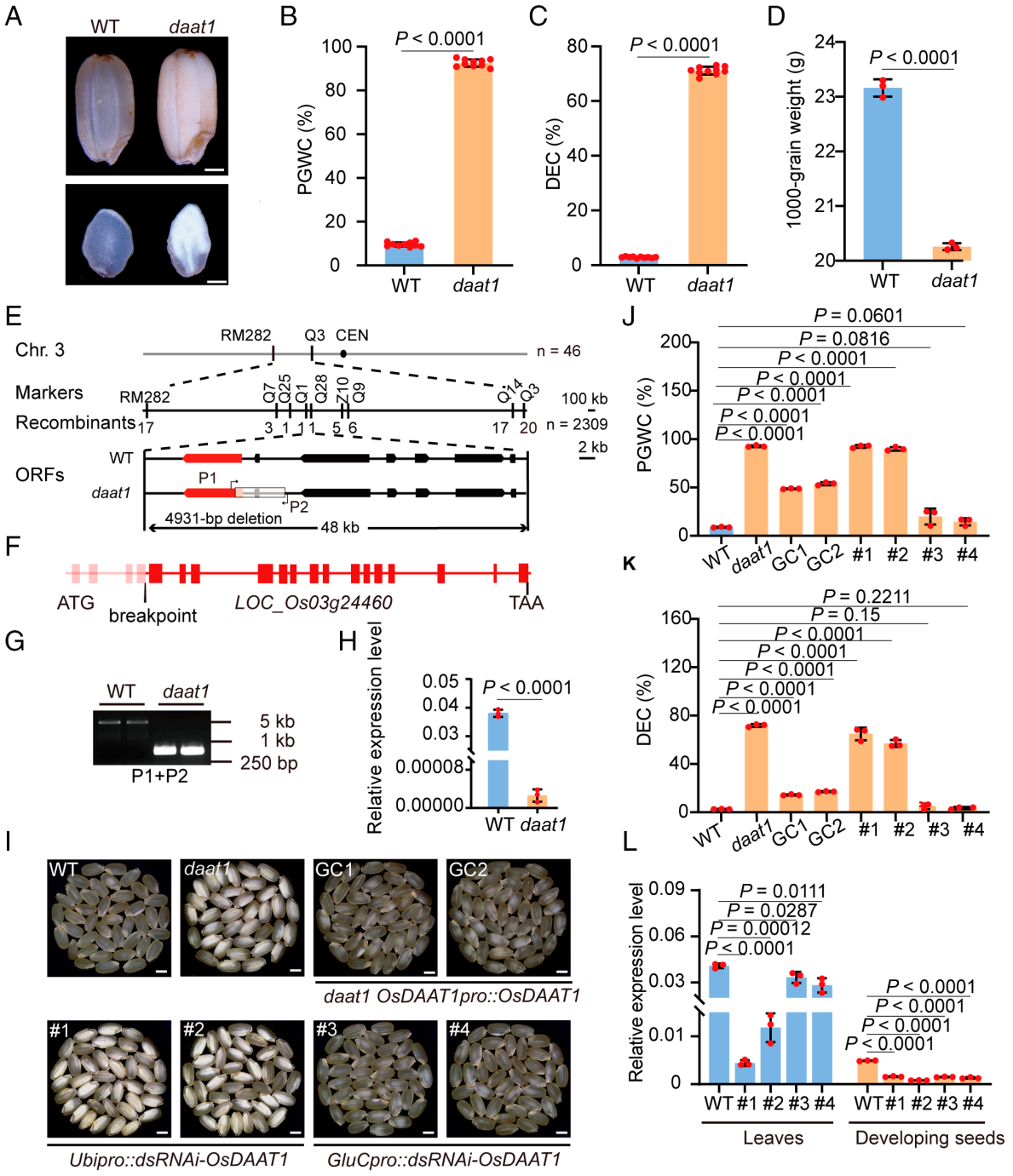

Fig. 1. Phenotypic characterization and Map-based cloning of *OsDAAT1*. (*A*) Mature grains of WT and *daat1*. (Scale bar, 1 mm.) (*B* and *C*) PGWC (*B*) and DEC (*C*), calculated as the average value of all grains from one plant. Values are means ± SD, n = 10. (*D*) 1,000-grain weight of WT and the *daat1* mutant. Values are means ± SD, n = 3. (*E*) Fine mapping mapped the *OsDAAT1* locus to a 48-kb region between markers Q1 and Q28 on rice chromosome 3 (Chr. 3). The molecular markers and numbers of recombinants are indicated. Black and red arrows represent the ORFs, and red one is *LOC_Os03g24460*. Black ellipse represents the centromere. Semitransparent rectangular frame represents a 4,931-bp deletion in *daat1* mutant. (*F*) Gene structure of *LOC_Os03g24460*. Red boxes represent exons, and lines represent introns. The pink shaded area indicates the genomic coding region deletion found in *daat1*. ATG and TAA represent the translation start and stop codons, respectively. (*G*) PCR analyses of the 4,931-bp deletion between WT and *daat1* mutant. P1 and P2 in (*G*) are the primers used for the PCR. (*H*) Relative expression levels of *OsDAAT1* in WT and the *daat1* mutant. Rice *Ubiquitin1* (*Os03g0234200*) was used as an internal control. (*I*) Mature grains of the WT, *daat1*, *OsDAAT1pro:OsDAAT1* [genomic complementation (GC) transgenic lines, GC1 and GC2], *Ubipro:dsRNAi-OsDAAT1* (#1 and #2) and *GluCpro:dsRNAi-OsDAAT1* (#3 and #4) plants. (Scale bar, 2.5 mm.) (*J* and *K*) PGWC (*J*) and DEC (*K*) of WT, *daat1*, *OsDAAT1pro:OsDAAT1* (GC1 and GC2), *Ubipro:dsRNAi-OsDAAT1* (#1 and #2) and *GluCpro:dsRNAi-OsDAAT1* (#3 and #4). (*L*) Relative expression levels of *OsDAAT1* in leaves and developing seeds at 9 DAF in the WT, *Ubipro:dsRNAi-OsDAAT1* (#1 and #2), and *GluCpro:dsRNAi-OsDAAT1* (#3 and #4) plants. Rice *Ubiquitin1* was used as an internal control. Three independent biological replicates were performed for each sample. *P* values were derived by Student's *t* test.

authentic standard D-amino acids by liquid chromatography/mass spectrometry (LC/MS) and found that D-Glu, D-Ala, D-Met, and D-Ser produced dominant ion peaks at *m/z* 428.142, 370.136, 430.140, and 386.131 $[M\text{-}H]^-$, respectively (*SI Appendix*, Fig. S6). We then performed an in vitro enzymatic assay of OsDAAT1. As a result, the peak of D-Ala was detected when D-Glu, D-Met, and D-Ser served as amino group donors, with pyruvate as an amino group acceptor (Fig. 2 *G* and *H* and *SI Appendix*, Fig. S7 *B–D*).

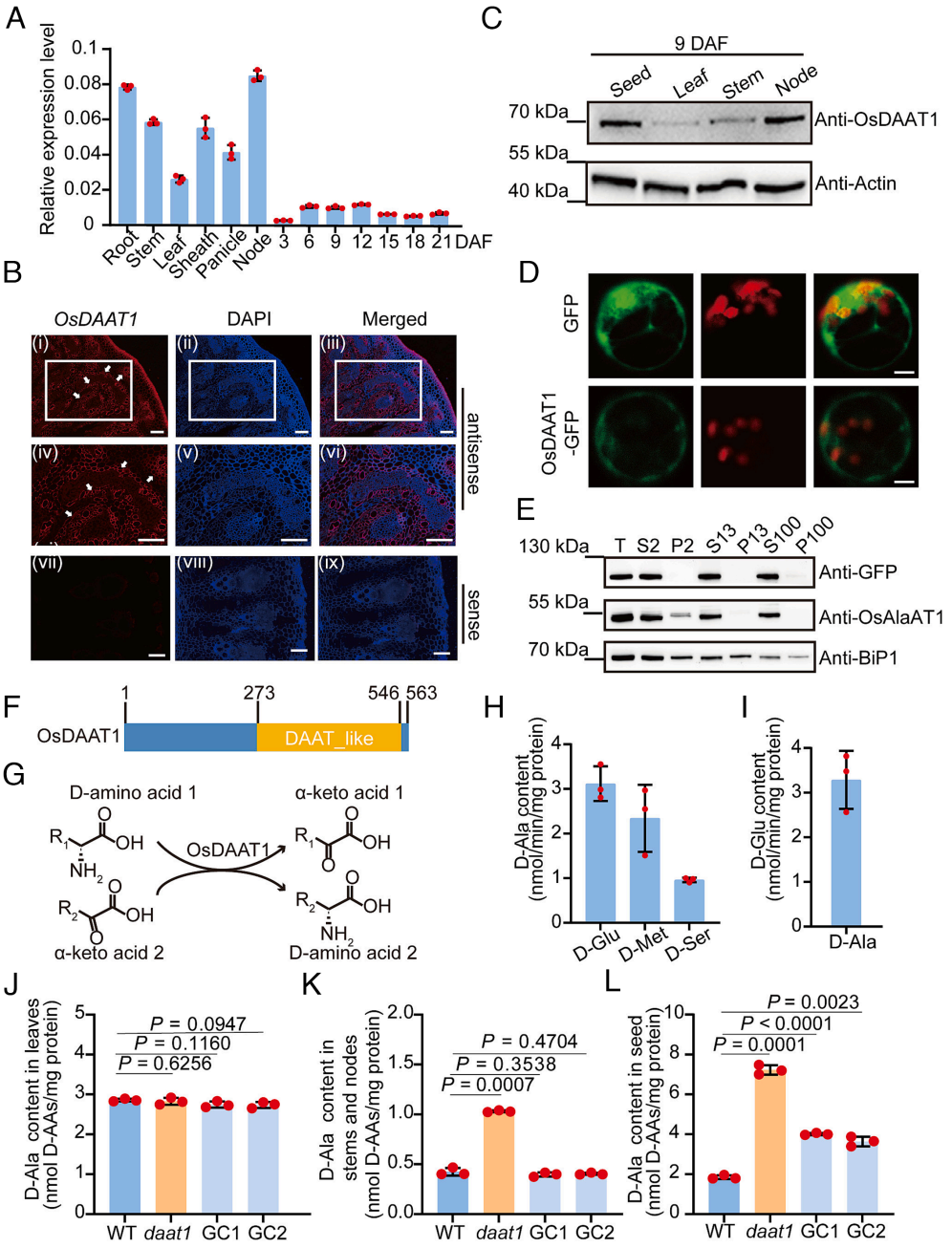

Fig. 2. *OsDAAT1* encodes a D-amino acid aminotransferase. (*A*) Relative expression levels of *OsDAAT1* in various plant tissues and developing seeds at the indicated DAF. Rice *Ubiquitin1* (*Os03g0234200*) was used as an internal control. Values are means ± SD, n = 3. (*B*) Expression pattern of *OsDAAT1* analyzed by in situ hybridization in the first node, as indicated by the red dotted line in (*SI Appendix*, Fig. S4*A*). Red signals indicate *OsDAAT1* transcripts detected by the antisense probe. The sense probe was used as a negative control. Nuclei were stained with DAPI (blue). Panels (*iv*–*vi*) represent magnified views of the boxed areas in (*i*–*iii*) respectively. Arrows in (*i*) and (*iv*) of (*B*) indicate the vascular tissues of the node. (Scale bar, 100 μm.) (*C*) Immunoblot analysis of OsDAAT1 protein levels in developing seed, leaf, stem, and node at 9 DAF. Anti-Actin was used as a loading control. (*D*) Subcellular localization of OsDAAT1 in protoplasts isolated from the *daat1 35Spro:OsDAAT1-GFP* plants. (Scale bar, 5 μm.) (*E*) Immunoblot analysis of subcellular fractions. T, total extract; S, supernatant; P, pellet. Numbers (2, 13, 100) indicate centrifugation speeds (×1,000 g). Anti-BiP1 and Anti-OsAlaAT1 were used as markers for the endoplasmic reticulum and cytoplasm, respectively. (*F*) Schematic representation of the domain structure of the OsDAAT1 protein. OsDAAT1 contains a predicted DAAT-like domain with 274 amino acid residues. (*G*) Diagram illustrating the transamination reaction catalyzed by OsDAAT1. (*H* and *I*) In vitro enzymatic activity of recombinant OsDAAT1 protein. Assays measured the transamination rates using different D-amino acids (D-Glu, D-Met, D-Ser) as donors to produce D-Ala (*H*), or using D-Ala to produce D-Glu (*I*). Values are means ± SD, n = 3. (*J*–*L*) Measurement of endogenous D-Ala content in leaves (*J*), stems and nodes (*K*), and seeds (*L*) of WT, *daat1* mutant, and GC transgenic lines (GC1 and GC2). Values are means ± SD, n = 3. *P* values were derived by Student's *t* test.

Moreover, D-Glu was produced when D-Ala served as an amino group donor and α-ketoglutarate as an amino group acceptor (Fig. 2*I* and *SI Appendix*, Fig. S7*A*). These results establish OsDAAT1 as a broad-spectrum D-amino acid aminotransferase in vitro.

We next quantified D–amino acids and found that only D-Ser and D-Ala can be detected in rice tissues (Fig. 2 *J*–*L* and *SI Appendix*, Fig. S7 *E*–*G*). In leaves, D-Ala and D-Ser levels were comparable among WT, *daat1*, and GC lines (Fig. 2*J* and *SI Appendix*, Fig. S7*E*). In stems and node, *daat1* showed increased D-Ala but reduced D-Ser compared with WT and GC lines (Fig. 2*K* and *SI Appendix*, Fig. S7*F*). In developing seeds, D-Ala was markedly elevated in *daat1*, whereas D-Ser levels were similar to WT and *daat1*. D-Ala was reduced in the GC line but remained higher than in WT (Fig. 2*L* and *SI Appendix*, Fig. S7*G*), possibly

reflecting the mixed maternal and filial origin of seed tissues. These results indicate that *OsDAAT1* mutation disrupts D-amino acid homeostasis, particularly in stems and node, supporting a maternal contribution to the chalky grain phenotypes.

***OsDAAT1* Mutation Induced ER Stress Response during Grain Development.** The period from 6 to 20 days after fertilization (DAF) is the key stage for aleurone and starchy endosperm differentiation, as well as for storage product accumulation during endosperm development in rice (27). To investigate the underlying cause of chalky grain formation in the *daat1* mutant, an RNA-Sequencing (RNA-Seq) was performed with 9-DAF developing seeds of WT and *daat1*. A total of 5,899 differentially expressed genes (DEGs) were identified ($|\log_2\text{Ratio}| \geq 0$; $P < 0.05$), including 3,436 up-regulated and 2,463 down-regulated genes (*SI Appendix*, Fig. S8*A* and Dataset S1 *A–B*). Kyoto Encyclopedia of Genes and Genomes (KEGG) pathway enrichment analysis revealed that these DEGs were predominantly involved in pathways such as ribosome function, carbon metabolism, starch and sucrose metabolism, and protein processing in the ER (Fig. 3*A*, *SI Appendix*, Fig. S8*B*, and Dataset S1 *C–V*). Notably, genes related to ER-stress were extensively upregulated in *daat1* and further RT-qPCR verified this result (Fig. 3 *A* and *B* and *SI Appendix*, Fig. S9). Western blotting verified a significant increase in the accumulation of ER-resident chaperone proteins in *daat1* (Fig. 3*C*). Additionally, transmission electron microscopy (TEM) analysis clearly showed swelling and aberrant ER structures in *daat1* developing endosperm cells (Fig. 3*D*), indicating a dysfunction of the ER. Considering that severe grain chalkiness in rice is closely associated with ER stress during endosperm development (4), these results collectively demonstrate that mutation of *OsDAAT1* induces severe ER stress, which may in turn impair endosperm development, ultimately leading to grain chalkiness in rice.

Given that the *OsDAAT1* mutation disrupts D-amino acid homeostasis and may induce severe ER stress in rice, we next investigated whether there is a functional connection between them. We initially injected a fluorescent D-Ala analogue (HADA) into the second internode of WT at 9 DAF and detected its accumulation in developing seeds after 24 h, suggesting that exogenous D-amino acids can be transported to seeds in rice (*SI Appendix*, Fig. S10). Subsequently, we independently injected D-Ala, D-Ser, and D-Met and analyzed the expression levels of ER stress-related genes in endosperm cells. While minimal changes were observed in transcript levels 1 h postinjection, significant upregulation was detected after 3 h (Fig. 3*E* and *SI Appendix*, Fig. S11*A*).

Furthermore, we treated 1-wk-old WT seedlings grown hydroponically with D-Ala, D-Ser, and D-Met, respectively. One hour after treatment, the transcription levels of ER stress-related genes were significantly increased compared to the negative control (*SI Appendix*, Fig. S11*B*). However, the elevated expression levels were further partially recovered after 3 h (*SI Appendix*, Fig. S11*C*). Together, these results demonstrate that exogenous D-amino acids can induce the expression of ER stress-related genes in both seedlings and developing grains, further suggesting that the overaccumulated D-amino acids in *daat1* may trigger a constitutive ER stress response.

***OsDAAT1* Mutation Altered the Protein Isomerization Levels and Extent.** Proteins are generally composed of L-amino acids; however, peptides and proteins containing D-amino acids have been reported in bacteria and animals (28, 29). Notably, even a single D-amino acid substitution can substantially alter protein isomerization and higher-order structure, thereby affecting protein function (30). Whether such D-amino acid–containing peptides/proteins exist in plants and whether their isomerization is influenced by perturbed D-amino acid metabolism remain unclear. To address this question, we performed a mass spectrometry-based proteomic analysis of total protein from 9-DAF seeds of WT, *daat1*, and GC transgenic line (Fig. 4*A* and Dataset S2 *A–M*). Initial quality assessment of the acquired data, including total ion chromatograms (TIC) (*SI Appendix*, Fig. S12), showed high reproducibility and data quality. The identified protein abundances spanned six orders of magnitude (*SI Appendix*, Fig. S13*A* and Dataset S2*L*), with peptide sequence coverage distributions indicative of comprehensive proteome capture (*SI Appendix*, Fig. S13*B* and Dataset S2*M*). The majority of identified peptides fell within the optimal length range of 7 to 25 amino acids (*SI Appendix*, Fig. S13*C* and Dataset S2*K*), confirming an efficient enzymatic digestion. Furthermore, high peptide identification confidence was achieved, with over 95% of peptides exhibiting scores above 50 (*SI Appendix*, Fig. S13*D* and Dataset S2*K*).

Traditional proteomic workflow enabled the identification of 2,089 proteins in WT, 2,272 proteins in *daat1* and 2,100 in GC transgenic line, with 1,853 proteins shared across all three groups, while 213 unique proteins (~9.4%, 213/2,272) were specific to *daat1* (Venn diagram, Fig. 4*B* and *SI Appendix*, Dataset S2*C*). Using a home-customized isomeric retrieval algorithm, we identified 156 isomerized proteins in WT, 177 in *daat1* and 159 in GC, with 110 proteins exhibiting isomerization in all genotypes (Venn diagram, Fig. 4*C* and *SI Appendix*, Dataset S2*E*). Similarly, we identified 8,425 peptides in WT, 9,709 peptides in *daat1* and 8,548 in GC transgenic line, with 4,308 peptides common to all datasets and 1,538 unique peptides (~15.8%, 1538/9709) in *daat1* (Venn diagram, Fig. 4*B* and *SI Appendix*, Dataset S2*D*). Using the isomeric retrieval algorithm, we identified 433 isomerized peptides in WT, 495 in *daat1* and 485 in GC, with 256 shared among three genotypes (Venn diagram, Fig. 4*C* and *SI Appendix*, Dataset S2*F*).

Notably, after isomeric screening, the number of unique proteins and peptides in *daat1* is 42 (~23.7%, 42/177) and 129 (~26.1%, 129/495), respectively, representing a significant enhancement in identification percentages compared to those without isomeric screening (~9.4% for proteins and ~15.8% for peptides, Fig. 4*C*). This approximately twofold increase in unique protein and peptide identification suggests the effectiveness of stereoproteome analysis, which substantially enhances proteomic coverage depth and resolution sensitivity, thereby providing a more reliable analytical framework for precise comparisons between WT and mutant strains. Taken together, our results clearly demonstrate that like in animals, plants also harbor D-amino acid-containing peptides/proteins. Although *daat1* displayed slightly higher overall protein isomerization levels and sequence STEP ratios, the differences were not statistically significant compared with those in WT and GC lines (Fig. 4 *D* and *E* and *SI Appendix*, Dataset S2 *G–H*).

Further quantitative analysis of isomerization regions revealed 10 significantly upregulated and 14 significantly downregulated peptides in WT vs. *daat1* and 19 significantly upregulated and 12 significantly downregulated peptides in GC vs. *daat1* (Fig. 4*F* and *SI Appendix*, Dataset S2*J*). Notably, heatmap analysis showed that isomerization levels of peptides derived from several functional proteins were significantly altered in *daat1* but restored to near-WT levels in GC line, such as A1YQG3 (Glutelin), Q10LT1 (Cupin family protein), Q67IX6 Protein disulfide isomerase (PDI), and various seed storage proteins (SSPs) (Fig. 4*G* and *SI Appendix*, Dataset S2*I*). Principal component analysis (PCA) further grouped WT and GC samples into a single cluster, clearly separating them from *daat1*, indicating that GC treatment effectively compensates for isomerization disturbances caused by *daat1* deficiency (Fig. 4*H* and *SI Appendix*, Dataset S2*I*). The results suggest that the loss of *daat1* may alter the higher-order structure of SSPs and PDI by affecting the isomerization modification.

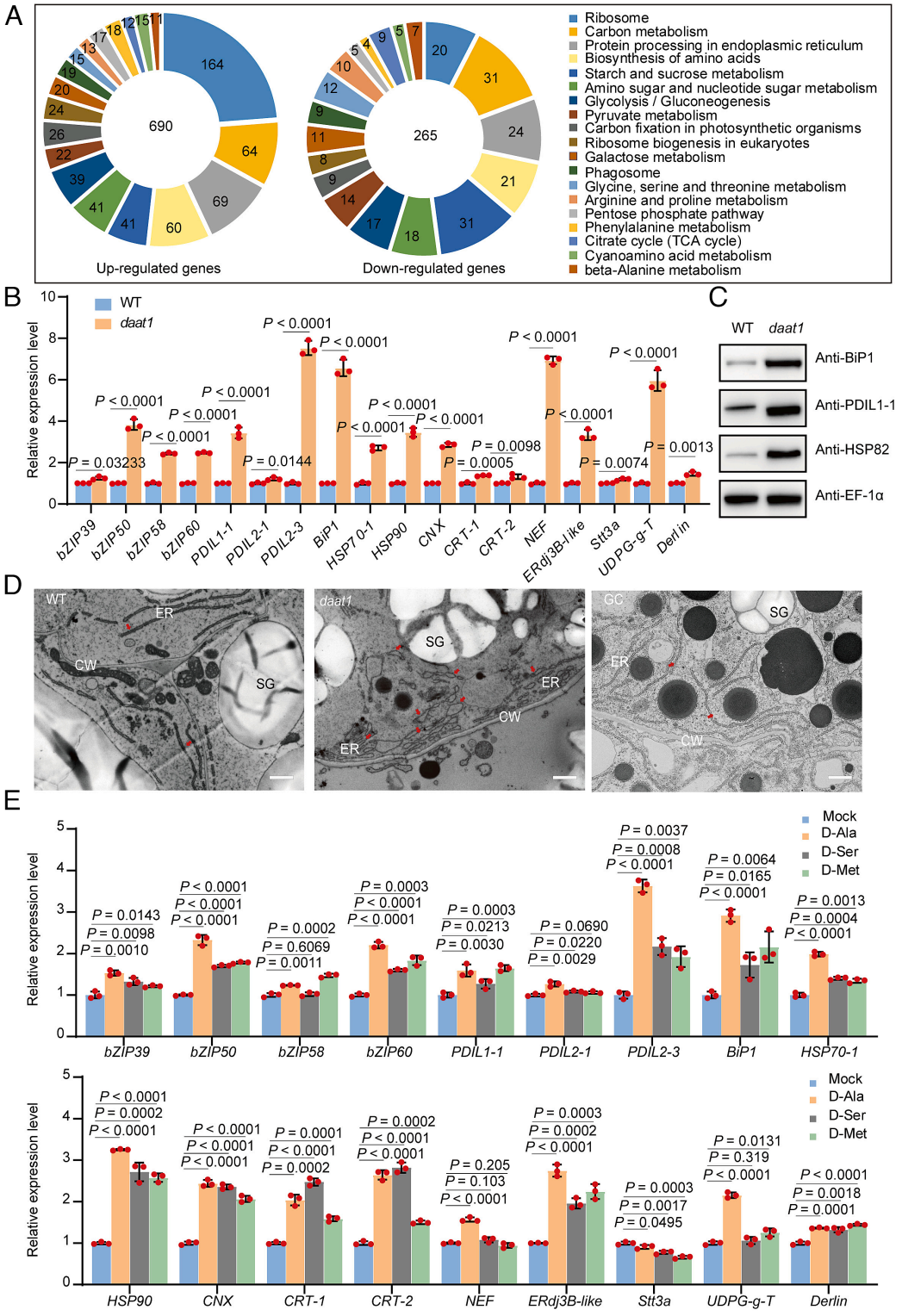

Fig. 3. Severe ER stress was induced in the *daat1* mutant. (*A*) The *Left* and *Right* panels show the number of up-regulated and down-regulated genes, respectively, in each KEGG pathway in the *daat1* mutant compared to the WT. (*B*) Validation of ER stress-related gene expression in WT and *daat1* through RT-qPCR analysis. Rice *Ubiquitin1* (*Os03g0234200*) was used as an internal control. The expression level of each gene in WT was normalized to 1. Values are means ± SD, n = 3. (*C*) Immunoblot analysis of ER stress markers BiP1, PDIL1-1, and HSP82. EF-1α was used as the loading control. (*D*) TEM images of endosperm cells in WT, *daat1* mutant, and GC transgenic lines at 9 DAF. ER, endoplasmic reticulum; SG, starch grain; CW, cell wall. Red arrows indicate the abnormal structures of ER lumen. (Scale bar, 1 μm.) (*E*) Relative expression levels of ER stress-related genes in developing seeds of WT at 9 DAF after being treated with exogenous D-amino acids for 3 h. The expression level of each gene in water-treated seeds was set to 1. Values are means ± SD, n = 3. *P* values were derived by Student's *t* test.

Natural Variations in *OsDAAT1* Promoter Region Associate with Grain Chalkiness. To access the contribution of natural variations in *OsDAAT1* to rice grain chalkiness, nucleotide polymorphisms in the *OsDAAT1* CDS and in regions ranging from 2,296 bp upstream of the ATG to 2,688 bp downstream of the TAA were investigated among 536 rice germplasms (*SI Appendix* Dataset S3). 16 single-nucleotide polymorphisms (SNPs) significantly associated with grain chalkiness were detected, including seven in the promoter,

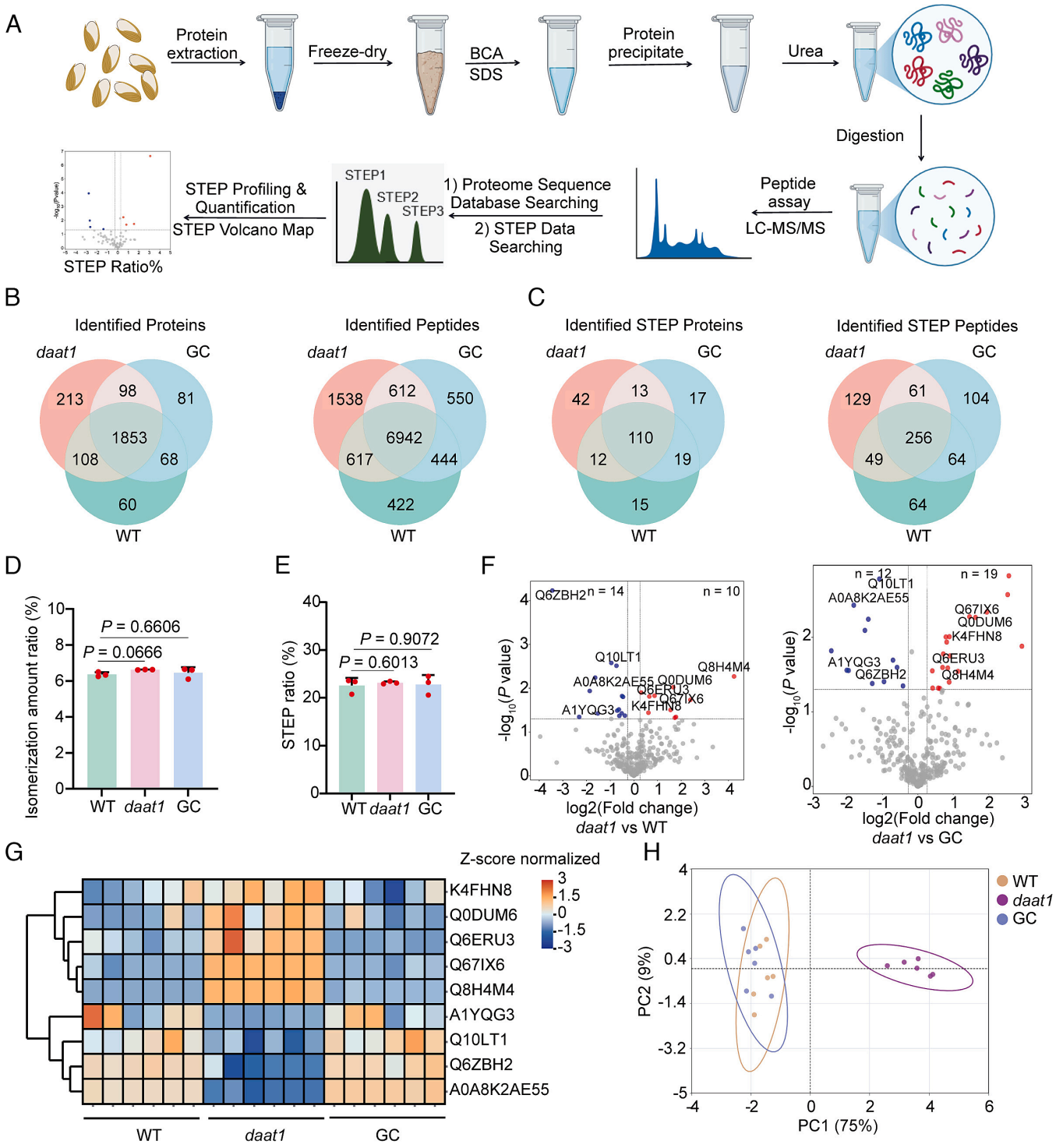

Fig. 4. Proteomic analysis of isomeric proteins with 9-DAF developing seeds of WT, *daat1*, and GC transgenic line. (*A*) Workflow for the proteomic analysis of protein isomerization. (*B* and *C*) Venn diagrams showing the overlap of total identified proteins and peptides (*B*) and identified STEP proteins and peptides (*C*) among WT, *daat1*, and GC transgenic lines. (*D* and *E*) Identification number-based calculation for the isomerization amount ratios at the protein level (*D*) and STEP ratio at the peptide level (*E*) across WT, *daat1*, and GC transgenic lines. Values are means ± SD, n = 3. *P* values were derived by Student's *t* test. (*F*) Volcano plots displaying the Fold changes (FC) in peptide isomerization ratios in *daat1* vs. WT (*Left*) and *daat1* vs. GC (*Right*). Red and blue dots represent significantly upregulated and downregulated peptides respectively. (*G*) Differential isomerization heatmap at the peptide level identified in (*F*). The color scale represents the normalized abundance (Z-score), ranging from low (blue) to high (orange). (*H*) PCA of differences in peptide isomerization levels identified in (*F*). The *daat1* mutant forms a distinct cluster, while the GC line clusters closely with the WT. FC in panels *F* represent the ratios of isomerization level of *daat1* sample to that of WT sample for the given peptides. Significant changes are defined by FC > 1.2 and $P < 0.05$. Source data for panels *B* and *C* are provided (n = 6). The data represent three independent biological replicates, each measured with two technical replicates to assess methodological stability. *P* values were derived by Student's *t* test.

one in the exon, five in the introns, one in the 3'untranslated region and two in the downstream regions (*SI Appendix*, Fig. S14*A*). Further analysis revealed that the SNP in the exon did not cause any amino acid change, but the seven SNPs in the promoter may lead to changes in putative transcription factor binding sites, such as the Anaerobic Response Element box and CAAT box

(Fig. 5*A* and *SI Appendix*, Fig. S14*A*). Based on the seven SNPs, two haplotypes were classified (Fig. 5*A*). Hap1 was identified as the elite haplotype associated with significantly lower PGWC and DEC compared to Hap2 (Fig. 5 *B* and *C* and *SI Appendix*, Fig. S14 *B* and *C*). Notably, Hap1 was predominantly found in *Aus/boro*, *Basmati/sadri*, *Geng/japonica* (*GJ*) and 62.7% of *Xian/Indica* (*XI*) accessions, while 37.3% of *XI* carried Hap2 (Fig. 5*A*). Further analysis using dual-luciferase reporter system showed that Hap1 conferred stronger transcriptional activation than Hap2 (Fig. 5*D*). Consistently, *OsDAAT1* expression levels were significantly higher in accessions with Hap1 than in those with Hap2 (Fig. 5*E* and *SI Appendix*, Fig. S14*D*). However, even higher levels of *OsDAAT1* by overexpressing $OsDAAT1^{Hap1}$ in Nipponbare (Hap1) did not lead to further reduction in grain chalkiness (*SI Appendix*, Fig. S15). To further assess the impact of these two haplotypes on grain chalkiness, we identified five chromosome segment substitution lines in the 9311 (Hap1 genotype) background harboring the *OsDAAT1* segment from PA64s (Hap2) (*SI Appendix*, Fig. S16). Phenotypic analysis revealed that introgression of the Hap2 allele resulted in a significantly higher PGWC across all five lines compared to the 9311 recurrent parent (Fig. 5 *F* and *G*). Taken together, natural variations in the *OsDAAT1* promoter region seem to regulate grain chalkiness by influencing *OsDAAT1* expression.

To examine whether *OsDAAT1* has been under artificial selection during rice domestication, we analyzed the genetic diversity of the *OsDAAT1* region using wild rice (*Oryza rufipogon* and *Oryza nivara*), landraces and Chinese cultivars (31). As a result, five haplotypes (Hap1 to Hap5) were identified in wild rice accessions and $OsDAAT1^{Hap1}$ is present in approximately 79.77% and 72.35% of *O.rufipogon* and *O.nivara*, respectively, suggesting that *OsDAAT1* underwent a bottleneck effect and became predominant in wild rice accessions (Fig. 5*H* and *SI Appendix*, Table S3). In contrast, only three haplotypes (Hap1, Hap2, and Hap4) were found in all the landraces and modern cultivars, indicating that *OsDAAT1* may be a selected target during rice domestication and breeding (Fig. 5*H*). Notably, the proportion of Hap1 increased dramatically in modern cultivars, reaching nearly 100%, which points to additional selective pressure on *OsDAAT1* (Fig. 5*H*). Further, we calculated the F_{ST} and nucleotide diversity (π) within a 2-Mb region surrounding the *OsDAAT1* locus in wild rice population. Our F_{ST} analysis revealed significant differentiation between *indica* and *japonica* (*SI Appendix*, Fig. S17*A*), while the π value of the *OsDAAT1* region was significantly lower in both *indica* and *japonica* compared to the wild rice varieties (*SI Appendix*, Fig. S17 *B* and *C*). These findings together suggest that *OsDAAT1* may have been artificial selected during rice domestication.

Discussion

DAATs of bacterial origin are stereospecific and exhibit activities toward a broad range of D-amino acids (32–35). Similarly, AtDAT1 also displays a broad range of D-amino acid substrates (18, 36). In our study, OsDAAT1 exhibits broad substrate activity for D-amino acids in vitro (Fig. 2 *G–I*). However, AtDAT1 also displays the different activity when using different amino group acceptors (18, 36). Among the tested substrates, the OsDAAT1 activity was slightly higher when D-Ala and D-Glu served as the amino donor (Fig. 2 *H* and *I*). While OsDAAT1 shares conserved pyridoxal 5'-phosphate (PLP)-binding residues with YM-1 DAAT and AtDAT1, variations in key substrate recognition residues likely dictate its distinct substrate preference (*SI Appendix*, Fig. S18). Further analysis showed that *OsDAAT1* mutation resulted in significantly elevated D-Ala content in stems, nodes, and developing seeds, while D-Ser content remained largely unchanged in developing seeds, but decreased in stems and node (Fig. 2 *K–L* and *SI Appendix*, Fig. S7 *E–G*). Previous study concluded that D-Ser is mainly synthesized by serine racemase, which converts L-Ser to D-Ser in *Arabidopsis* (19). Therefore, it can be inferred that OsDAAT1 is mainly involved in D-Ala metabolism rather than D-Ser metabolism in rice.

How do D-amino acids regulate ER homeostasis? Evidence suggests D-amino acids can be incorporated into nascent polypeptides via the translational machinery or arise from enzymatic posttranslational epimerization, altering protein stereochemistry (29, 37, 38). Therefore, these findings suggest that D-amino acids may compete with L-amino acids as the substrates for the translational machinery, leading to translation disorders during peptide elongation and alters protein isomerization. Consistent with this, we identified stereo-isomerized peptides and proteins in developing rice seeds, where *daat1* mutants displayed isomerization profiles distinct from WT and GC transgenic lines (Fig. 4). These findings support the hypothesis that perturbations in D-amino acid homeostasis contribute to altered levels of peptide and protein isomerization. Analogous to the D-amino acid–driven aggregation observed in Alzheimer's disease and amyotrophic lateral sclerosis (39, 40), we propose that such stereochemical alterations disrupt protein folding and processing in the ER, thereby triggering the unfolded protein response. Consistently, elevated D-Ala levels in *daat1* tissues coincided with severe ER stress, which is recapitulated in WT plants by exogenous D-amino acid treatment (Fig. 3 and *SI Appendix*, Figs. S8–S11). While these data suggest D-amino acid accumulation precipitates ER stress via protein misfolding, other indirect mechanisms cannot be ruled out. Cereal endosperm development is highly sensitive to ER stress, which impairs starch and protein deposition (4, 41). Consistently, *daat1* endosperm exhibited significantly reduced activities of starch synthase and ADP-glucose pyrophosphorylase, alongside altered expression of storage protein genes (Fig. 3*A* and *SI Appendix*, Figs. S8 and S20). Thus, the severe, constitutive ER stress in *daat1* likely contributes to grain chalkiness by disrupting the accumulation of storage reserves.

Generally, endosperm phenotypes are governed by three distinct genetic components: the zygotic effect arising from the endosperm's own genotype; the maternal sporophyte effect, which influences development through maternal tissues; and the cytoplasmic effect, derived from organelle genomes (mitochondria and chloroplasts) (42). Mutants with maternal sporophyte effects on seed development are revealed by significant reciprocal differences, and recessive maternal sporophyte effect mutants will only have consequences if parent plants are homozygous (43). Genetic analysis revealed that grain chalkiness in *daat1* is determined in a recessive maternal sporophyte manner, as the phenotype manifests only when the maternal plant is homozygous (*SI Appendix*, Fig. S2 and Table S2). This implies the defect lies in maternal tissues rather than in the zygotic endosperm. In addition, *OsDAAT1* is highly expressed in stems, nodes and vascular tissues, the homeostasis of D-amino acids is significantly disturbed in stems and nodes, with higher D-Ala and lower D-Ser. In leaves, both D-Ala and D-Ser are comparable between WT and *daat1*, while developing seeds showed elevated D-Ala without a significant change in D-Ser (Fig. 2 *A–C*, *J*, and *K* and *SI Appendix*, Figs. S4*A* and S7 *E–J*). Endosperm-specific silencing of *OsDAAT1* produces transparent grains, whereas constitutive silencing results in chalky grains. These results suppose that the expression pattern of *OsDAAT1* and the homeostatic of D-amino acids in these maternal tissues, especially in vascular tissue, disrupts metabolic homeostasis. The stems and nodes, especially nodes, function as the primary transport tissues. This phenomenon is reminiscent of the rice *GIF1* mutant, where defects in maternal vascular tissues impair nutrient transport, limiting grain filling (44).

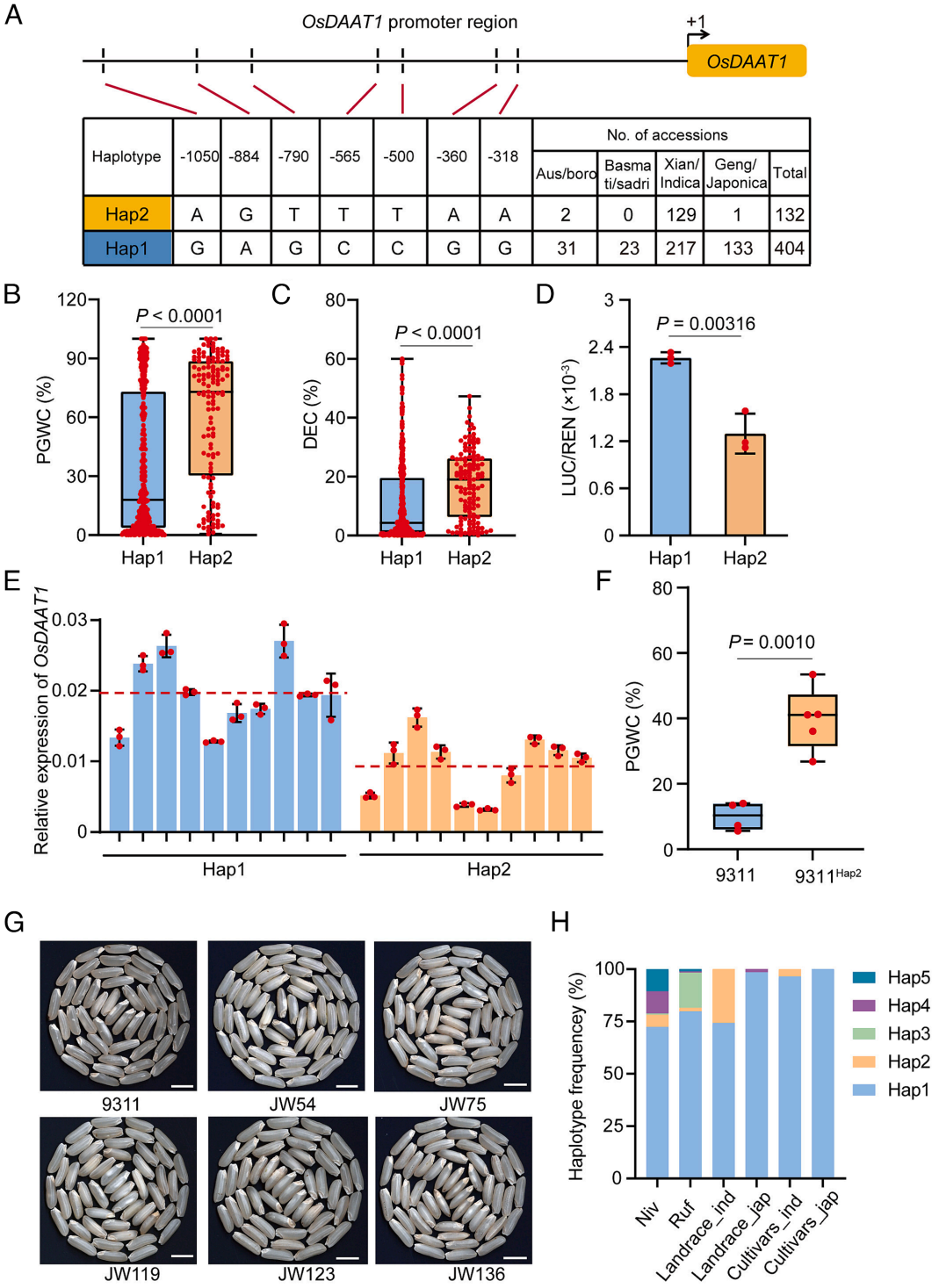

Haplotype	-1050	-884	-790	-565	-500	-360	-318	No. of accessions				
								Aus/boro	Basmati/sadri	Xian/Indica	Geng/Japonica	Total
Hap2	A	G	T	T	T	A	A	2	0	129	1	132
Hap1	G	A	G	C	C	G	G	31	23	217	133	404

Fig. 5. Haplotype analysis of *OsDAAT1* associated with grain chalkiness. (*A*) Natural variation and haplotype analysis of the *OsDAAT1* promoter region in 536 sequenced rice accessions. Numbers above the positions of variations relative to the putative translation start site ATG, (with the A of ATG designated as +1). (*B* and *C*) Comparison of PGWC (*B*) and DEC (*C*) between Hap1 and Hap2 in the 536 rice accessions. Values are means ± SD. (*D*) Transient expression assays of the two *OsDAAT1* promoter types in rice protoplasts. Values are means ± SD, n = 3. (*E*) Relative expression levels of *OsDAAT1* in representative rice varieties with Hap1 and Hap2 haplotypes. Red dotted lines represent the average expression levels of *OsDAAT1* in representative rice varieties. Rice *Ubiquitin1* (Os03g0234200) was used as the internal control. Values are means ± SD, n = 3. (*F*) Comparison of PGWC between *Indica* variety 9311 and 9311^{hap2} lines carrying Hap2 in the genetic background of the 9311. n = 4 for 9311, and n = 5 for 9311^{hap2} lines. (*G*) Representative images of brown rice grains from 9311 and 9311^{hap2} lines carrying Hap2 (JW series). (Scale bar, 5 mm.) (*H*) Haplotype frequencies are shown as percentages for a core collection of wild, landrace, and cultivated rice accessions. *P* values were derived by Student's *t* test.

Supporting this hypothesis, F_1 seeds from *daat1* (female) × WT crosses exhibit significantly higher D-Ala content than seeds from reciprocal crosses (*SI Appendix*, Fig. S19).

In conclusion, our results demonstrate that *OsDAAT1* maternally regulates grain quality by modulating D-amino acid metabolism, a process essential for maintaining ER homeostasis. Disruption of this pathway alters protein isomerization and triggers severe ER stress. While D-amino acid–containing peptides are documented in bacteria and animals (30, 45, 46), our study provides direct evidence for their existence and functional impact in plants.

Furthermore, the identification of the elite haplotype Hap1 offers a promising genetic resource for improving rice grain appearance.

Methods

Plant Materials and Growth Conditions. The *daat1* mutant was isolated from a tissue culture-induced mutant library of the *japonica* rice cultivar Nipponbare. The rice plants were grown at the Tuqiao experimental stations of Nanjing Agricultural University during the natural growing season in Nanjing, Jiangsu. During winter, plants were cultivated in Sanya, Hainan.

For exogenous D-amino acids treatment, rice seedlings were cultured in 96-well microtiter plates with half-strength Murashige and Skoog (MS) medium. The conditions in the growth cabinet alternate between 30 °C for 14 h under light and 28 °C for 10 h in the dark.

Microscopy. For scanning electron microscopy, dry seeds were transversely cut, sputter-coated with gold and scanned with a Hitachi S-3400 N scanning electron microscope (Hitachi, Japan) (47). For TEM and semithin section experiments, developing seeds were fixed, dehydrated, embedded, and examined according to the methods described previously (48).

Map-Based Cloning. To map the *daat1* locus, we constructed an F_2 mapping population derived from a cross between *daat1* and the *indica* cultivar N22. The locus was initially mapped to a region between the polymorphic SSR markers RM282 and Q3 on Chr. 3 using 46 F_2 mutant plants. For fine mapping, 2,309 recessive segregates were adopted to narrow the *daat1* locus to a 48 kb interval between the markers Q1 and Q28. Markers used in this study are listed in *SI Appendix*, Table S4.

Plasmid Construction and Rice Transformation. For genetic complementation test, the *OsDAAT1* CDS under its native promoter was cloned into the binary vector pCAMBIA1390 to generate *OsDAAT1pro:OsDAAT1* construct. To obtain *OsDAAT1* knockout lines, a 20-bp guide RNA (5′-CTTACCAAAGGATAACGGCG-3′) was cloned into the CRISPR/Cas9 vector as previously described (49).

To generate the *Ubipro:dsRNAi-OsDAAT1* construct, two inverted repeats of 168 bp were amplified from WT and sequentially cloned into LH-FAD2-1390RNAi in the antisense and sense orientations, using primers listed in *SI Appendix*, Table S4. To generate the *GluCpro:dsRNAi-OsDAAT1* construct, the *Glutelin C* (*GluC*) promoter was first cloned and inserted into LH-FAD2-1390RNAi empty vector to replace *Ubi* promoter. Then the same two inverted repeats were sequentially cloned into the intermediate vector in the antisense and sense orientations, using primers listed in *SI Appendix*, Table S5. These recombinant plasmids were transformed into Nipponbare calli by the *Agrobacterium*-mediated method (50).

Subcellular Localization and Fractionation. For subcellular localization, *OsDAAT1* CDS was cloned into pAN580 to produce *GFP-OsDAAT1* and *OsDAAT1-GFP* fusion constructs driven by the *CaMV 35S* promoter, using primers listed in *SI Appendix*, Table S4. The resulting constructs were individually transformed into rice protoplasts following previous description (51). After incubation for 16 h, the GFP-fused proteins were observed using a laser confocal microscope (Leica TCS SP8, Germany).

To generate the *35Spro:OsDAAT1-GFP* fusion construct, *OsDAAT1* CDS was cloned into the binary vector pCAMBIA1305-GFP, using primers listed in *SI Appendix*, Table S4. The resulting plasmid was transferred into the *daat1* calli by the *Agrobacterium tumefaciens*-mediated method (50). The protoplasts of the positive transgenic lines were isolated, examined with the same confocal microscope as described above.

For subcellular fractionation, 6-DAF endosperm samples were homogenized, filtered, and centrifuged to separate into the cytosolic and microsomal fractions as depicted previously (52). S2 and P2 indicates the supernatant (S2) and pellet fractions (P2) centrifuged at 2,000 g for 20 min. Then the S2 fraction was further centrifuged at 13,000 g to obtain the supernatant (S13) and pellet fractions (P13). Finally, the S13 fraction was further centrifuged at 1,00,000 g to obtain the supernatant (S100) and pellet fractions P100 for immunoblot analysis.

RNA Extraction and RT-qPCR Analysis. Total RNA was isolated with the RNA Prep Pure Plant Kit (TIANGEN Biotech) and digested with DNaseI following the manufacturer's instructions. First-strand cDNA was synthesized using the PrimeScript RT Reagent Kit (TaKaRa). RT-qPCR was performed with the SYBR Green I mix (TaKaRa) and the T100TM Real-time PCR system (Bio-Rad, United States). mRNA levels were calculated by the comparative CT method (53) and the rice *Ubiquitin1* gene was serving as the internal control. Primer sequences used for RT-qPCR analysis are listed in *SI Appendix*, Table S4.

In Situ Hybridization. The rice first node was prepared and fixed in formaldehyde-acetic acid-alcohol solution (a mixture of 70% ethanol, glacial acetic acid, and 38% formaldehyde at an 18:1:1 v/v ratio) at the initial heading stage. Then standard paraffin sections were prepared and in situ hybridization was performed according to published protocols with slight modifications (54). Single-stranded RNA oligonucleotide probe was labeled with red cyanine3 at the 5′ terminus (Cy3, 5′- CAGGUACUGGAAGAGGAGGAUCAGGUAAUGUUG -3′).

Expression and Purification of Recombinant Proteins. The *OsDAAT1* CDS was cloned into the pGEX-4 T-2 vector. The recombinant construct was transformed into *Escherichia coli* strain BL21 (*DE3*) and grown at 37 °C in LB medium containing 100 μg mL^{-1} ampicillin. When the OD_{600} reached 0.6, isopropyl β-D-thiogalactoside was added to a final concentration of 0.5 mM. The cells were then cultured for additional 24 h at 16 °C before harvesting. The GST-OsDAAT1 proteins were purified using the Glutathione MagBeads (GenScript, China) according to the manufacturer's protocol.

Enzyme Assays. The 1.0 mL mixture for the OsDAAT1 activity assay consisted of 100 mM potassium phosphate buffer (pH 8.0), 50 mM D-amino acids as an amino donor, 50 mM pyruvate as an amino acceptor, 50 μM PLP, and the GST-OsDAAT1 proteins (10 μg of proteins) (18). The mixture was incubated at 37 °C for 10 min, followed by an ice-bath for 10 min. After centrifugation and derivatization, the amount of D-Ala produced was determined through a LC/MS system (Xevo®; G2-XS QTof, Waters).

D-amino acids and HADA Treatment. One-week old seedlings and field-grown plants at the grain-filling stage were used for exogenous D-amino acids and HADA (a fluorescent D-Ala analogue, 7-hydroxycoumarin-3-amino-D-Ala, Tocris, 6647) treatments. First, 1-wk old seedlings were treated with water, 2 mM D-Ala, D-Ser, and D-Met respectively. The aboveground parts of these seedlings were harvested and immediately frozen in liquid nitrogen. Second, 0.5 mL water, 2 mM D-Ala, 2 mM D-Ser, 2 mM D-Met, and 0.1 mM HADA were separately injected into the second internode of field-grown plants at 9 DAF. Endosperm was harvested and immediately frozen 24 h postinjection. Three biological replicates were performed, and three tillers were used for each replicate.

Amino Acid Extraction, Derivatization, and Determination. For D-amino acids extraction, 1-wk old seedlings and 9-DAF endosperm were respectively homogenized in buffer (100 mM Tris-HCl, pH 8.0, and 1× complete protease inhibitor cocktail), followed by centrifugation to collect supernatant (55). The derivatization of amino acids in the plant extracts was performed according to the previous reports (55, 56).

The derivatives were then quantified by the Liquid Chromatograph Mass Spectrometer (LC-MS) system. Two microliters of the solution were injected into the ultra performance liquid chromatography (UPLC) column (2.1 × 100 mm ACQUITY UPLC BEH C18 column containing 1.7 μm particles) at a flow rate of 0.4 mL/min. Buffer A consisted of 0.1% formic acid in ultrapure H_2O, and buffer B consisted of 0.1% formic acid in acetonitrile. The gradient was as follows: 10% buffer B for 0.5 min, 10 to 90% buffer B for 11 min, and 95% buffer B for 2 min.

Mass spectrometry was performed using electrospray source in positive ion mode with MS acquisition. The selected mass range was 50 to 1,200 m/z, and the lock mass option was enabled using leucine-enkephalin (m/z 556.2771) for recalibration. The mass spectrometer was operated at a capillary voltage of 3,000 V, a cone voltage of 30 V, a source temperature of 120 °C, a desolvation gas temperature of 400 °C, and a collision energy of 20 to 40 eV. Data acquisition and processing were performed using Masslynx 4.1. Extraction of centroid spectra peaks with a width of 0.01 Da was used to determine the extracted ion chromatograms from the TIC.

RNA-Seq Analysis. Total RNA was extracted from 9-DAF developing endosperm of WT and *daat1* for library construction. Sequencing was performed on an Illumina Novaseq6000 platform by Gene Denovo Biotechnology Co. (Guangzhou, China). Approximately 2.5-Gb clean data were generated per sample and all clean reads

were mapped to the rice reference genome (GCF_001433935.1_IRGSP-1.0). To verify the transcript abundance calculated in RNA-seq, RT-qPCR analyses of ER stress related genes were performed using gene-specific primers (*SI Appendix*, Table S4).

Proteomic Analysis of Isomeric Proteins. Total protein extractions from 9-DAF developing endosperm of WT, *daat1* and GC were performed as described previously (52), followed by Surfactant and Coagulant Assisted Sequential Extraction/On-Particle Digestion proteomic method (57). Then samples were analyzed on ThermoFisher Orbitrap Fusion Lumos by Liquid Chromatograph Tandem Mass Spectrometry (LC-MS/MS) according to the previously reported method (57). The MS proteomics data have been deposited to the ProteomeXchange Consortium via the PRIDE partner repository with the dataset identifier PXD059692.

Protein identification and quantification were performed using MaxQuant (version1.6.3.4). Raw files were searched against the *Oryza sativa* subsp. *japonica* reviewed database with trypsin/P selected as the enzyme. For MS^1 scans, a precursor ion mass tolerance of 10 ppm was used, and two missed cleavages were allowed. Fragment ion tolerance was set to 0.02 Da for the Orbitrap MS^2 detections and 0.5 Da for the IT detections. The false discovery rate was set to 1% for both protein and peptide identification by the target decoy strategy. Carbamidomethylation of cysteine residues (+57.02146 Da) was chosen as the fixed modification, and variable modification included oxidation of methionine residues (+15.99492 Da) and acetylation at protein N termini (+42.01056 Da). The quantification method was set to MaxLFQ algorithm and protein quantitative ratios were determined using a minimum of two quantified peptides. All other parameters were set as default.

All statistical analyses were accomplished and filtered for reverse proteins, proteins only identified by site and potential contaminants were excluded from the identification list by Perseus (version 1.6.14.0). The dataset was further analyzed and two-sample Student's *t* test with a two-tailed distribution and one-way ANOVA were also performed. All *P*-values were further subjected to multiple testing corrections using the Benjamini–Hochberg method. Venn diagrams and volcano plots were generated using the Bioinformatics online platform (https://www.bioinformatics.com.cn).

As recently reported (58), the isomeric proteins were identified by using a sequence-guided data-searching algorithm for identified peptide ions of the same amino acid sequences/molecular weights but with varied LC retention times (RT), and the ratio_D (defined as the isomerization level, through excluding the fraction of L-counterparts) was calculated based on the peak intensities outputted by MaxQuant software. Specifically, the process is as follows: First, rows with zero or empty Intensity values are filtered out to remove invalid data. The data are then grouped by sequence and charge. Low-intensity charge information is eliminated to ensure distinct primary charge peaks for each sequence. Rows with a relative RT difference of less than 0.5% and low intensity are excluded to remove isotope peaks and abnormal tailing peaks. Next, the relative proportions of the target peaks within each sequence are calculated. False-positive noise (ratio < 1%) is removed. The ratios are then recalculated to determine the isomerization ratio and the number of isomers per sequence. Finally, a concise list of isomeric modifications is generated, containing the protein/gene name, sequence, charge, m/z, RT, collision cross section, intensity, and isomer ratio.

All codes used in this study are available on GitHub (https://github.com/limslab/STEP_Search.git).

Haplotype Analyses and Nucleotide Diversity Estimation. Sequence variation spanning 2,296 bp upstream of translation start codon ATG to 2,688 bp downstream of translation start codon TAA of *OsDAAT1* was identified and used for haplotype analysis based on 536 rice germplasm accessions (*SI Appendix*, Dataset S3). For evolutionary analysis of *OsDAAT1*, genomic sequences were obtained from a total of 2,509 accessions, including 343 wild rice and 909 landraces from Jing et al. (31), as well as 624 *indica* cultivars and 633 *japonica* cultivars from our Lab. Nucleotide diversity (π) and fixation index (*Fst*) for *OsDAAT1* and its flanking regions (about 2 Mb) were calculated for each rice group by VCFtools software (http://vcftool.github.io/) using a 100 kb window with a step size of 5 kb.

Data, Materials, and Software Availability. RNA-seq data have been deposited in NCBI Sequence Read Archive under accession number PRJNA1426511 (59). Proteomic data have been deposited in PRIDE under identifier PXD059692 (60). Study data are included in the article and/or supporting information.

ACKNOWLEDGMENTS. We thank Prof. Ling Jiang for providing the *wsd1* mutant and wild-type N22 seeds. This research was supported by grants from the National Key Research and Development Program of China (2023ZD0406902 and 2022YFA1305200), National Natural Science Foundation of China (22474062, 31971908, and 31830064), the "JieBangGuaShuai (JBGS)" Project of Seed Industry Revitalization in Jiangsu Province [JBGS (2021) 008 and JBGS (2021) 035], the Open Funds of the State Key Laboratory of Crop Genetics & Germplasm Enhancement and Utilization (ZW202403). The work was also supported by the Key Laboratory of Biology, Genetics, and Breeding of *japonica* Rice in Mid-lower Yangtze River, Ministry of Agriculture, Peoples Republic of China, Jiangsu Collaborative Innovation Center for Modern Crop Production and Haihe Laboratory of Sustainable Chemical Transformation.

Author affiliations: [a]State Key Laboratory of Crop Genetics and Germplasm Enhancement and Utilization, Zhongshan Biological Breeding Laboratory, Jiangsu Nanjing Rice Germplasm Resources National Field Observation and Research Station, Nanjing Agricultural University, Nanjing 210095, China; [b]Tianjin Key Laboratory of Biosensing and Molecular Recognition, Research Center for Analytical Science, Frontiers Science Center for New Organic Matter, College of Chemistry, Nankai University, Tianjin 300071, China; [c]College of Life Sciences, Nanjing Agricultural University, Nanjing 210095, China; and [d]State Key Laboratory of Crop Gene Resources and Breeding, National Key Facility for Crop Gene Resources and Genetic Improvement, Institute of Crop Sciences, Chinese Academy of Agricultural Sciences, Beijing 100081, China

Author contributions: H.D., Y.T., G.L., Y.W., and J.W. designed research; H.D., J. Lei, J. Liu, H.Y., X.J., R.Z., Yu Zhang, R.C., F.L., Y.R., Y.L., X.L., S.L., X.Y., Y.W., C.G., Yipeng Zhang, X.C., Yunpeng Zhang, H.X., and R.S. performed research; H.D., J. Liu., X.X., R.L., and G.L. contributed new reagents/analytic tools; H.D., J. Lei, J. Liu, X.J., Y.B., E.D., X.T., and G.L. analyzed data; Y.T. supervised this research; and J.L. wrote the paper.

The authors declare no competing interest.

1. L. Chen *et al.*, Genes controlling grain chalkiness in rice. *Crop J.* **12**, 979–991 (2024).
2. K. Kaneko *et al.*, Proteomic and glycomic characterization of rice chalky grains produced under moderate and high-temperature conditions in field system. *Rice* **9**, 1–16 (2016).
3. Y. B. Li *et al.*, *Chalk5* encodes a vacuolar H^+-translocating pyrophosphatase influencing grain chalkiness in rice. *Nat. Genet.* **46**, 398–404 (2014).
4. W. Yang *et al.*, *OsbZIP60*-mediated unfolded protein response regulates grain chalkiness in rice. *J. Genet. Genomics* **49**, 414–426 (2022).
5. B. Wu *et al.*, Natural variation in *WHITE-CORE RATE 1* regulates redox homeostasis in rice endosperm to affect grain quality. *Plant Cell* **34**, 1912–1932 (2022).
6. X. L. Chen *et al.*, Natural variation in *OsTPS8* confers differential regulation of chalkiness and seed vigor in indica and japonica rice. *Nat. Genet.* **58**, 206–217 (2025), 10.1038/s41588-025-02429-2.
7. A. D'Aniello, D-aspartic acid: An endogenous amino acid with an important neuroendocrine role. *Brain Res. Rev.* **53**, 215–234 (2007).
8. L. Pollegioni *et al.*, D-amino acids: New functional insights. *FEBS J.* **292**, 4395–4417 (2025), 10.1111/febs.70083.
9. J. T. Park, J. L. Strominger, Mode of action of penicillin. *Science* **125**, 99–101 (1957).
10. R. Konno *et al.*, *D-Amino Acids: A New Frontier in Amino Acids and Protein Research-Practical Methods and Protocols* (Nova Biomedical Books, New York, 2007).
11. Y. Saitoh *et al.*, D-serine and D-alanine regulate adaptive foraging behavior in *Caenorhabditis elegans* via the NMDA receptor. *J. Neurosci.* **40**, 7531–7544 (2020).
12. X. Dai *et al.*, D-serine made by serine racemase in *Drosophila* intestine plays a physiological role in sleep. *Nat. Commun.* **10**, 1986 (2019).
13. H. Brückner, T. Westhauser, Chromatographic determination of L- and D-amino acids in plants. *Amino Acids* **24**, 43–55 (2003).
14. O. Forsum, H. Svennerstam, U. Ganeteg, T. Nasholm, Capacities and constraints of amino acid utilization in *Arabidopsis*. *New Phytol.* **179**, 1058–1069 (2008).
15. P. W. Hill *et al.*, Acquisition and assimilation of nitrogen as peptide-bound and D-enantiomers of amino acids by wheat. *PLoS One* **6**, e19220 (2011).
16. Y. Fujitani, T. Horiuchi, K. Ito, M. Sugimoto, Serine racemases from barley, *Hordeum vulgare* L., and other plant species represent a distinct eukaryotic group: Gene cloning and recombinant protein characterization. *Phytochemistry* **68**, 1530–1536 (2007).
17. G. A. Miura, S. E. Mills, The conversion of D-tryptophan to L-tryptophan in cell cultures of tobacco. *Plant Physiol.* **47**, 483–487 (1971).
18. M. Funakoshi *et al.*, Cloning and functional characterization of *Arabidopsis thaliana* D-amino acid aminotransferase-D-aspartate behavior during germination. *FEBS J.* **275**, 1188–1200 (2008).
19. E. Michard *et al.*, Glutamate receptor-like genes form Ca^{2+} channels in pollen tubes and are regulated by pistil D-serine. *Science* **332**, 434–437 (2011).
20. B. G. Forde, M. R. Roberts, Glutamate receptor-like channels in plants: A role as amino acid sensors in plant defence? *F1000Prime Rep.* **6**, 37 (2014).
21. E. B. Monselise, A. Levkovitz, D. Kost, Ultraviolet radiation induces stress in etiolated *Landoltia punctata*, as evidenced by the presence of alanine, a universal stress signal: A ^{15}N NMR study. *Plant Biol.* **17** (suppl. 1), 101–107 (2015).
22. T. Hirano *et al.*, Moss chloroplasts are surrounded by a peptidoglycan wall containing D-amino acids. *Plant Cell* **28**, 1521–1532 (2016).

23. Ü. Kolukisaoglu, D-amino acids in plants: Sources, metabolism, and functions. *Int. J. Mol. Sci.* **21**, 5421 (2020).
24. R. B. Goldberg, G. Paiva, R. Yadegari, Plant embryogenesis: Zygote to seed. *Science* **266**, 605–614 (1994).
25. Y. S. Huang *et al.*, WEAK SEED DORMANCY 1, an aminotransferase protein, regulates seed dormancy in rice through the GA and ABA pathways. *Plant Physiol. Biochem.* **202**, 107923 (2023).
26. M. S. Zhong *et al.*, *Floury endosperm12* encoding alanine aminotransferase 1 regulates carbon and nitrogen metabolism in rice. *J. Plant Biol.* **62**, 61–73 (2019).
27. J. X. Liu, M. W. Wu, C. M. Liu, Cereal endosperms: Development and storage product accumulation. *Annu. Rev. Plant Biol.* **20**, 255–291 (2022).
28. C. Ollivaux, D. Soyez, J. Y. Toullec, Biogenesis of D-amino acid containing peptides/proteins: Where, when and how? *J. Pept. Sci.* **20**, 595–612 (2014).
29. A. M. Torres *et al.*, D-amino acid residue in the C-type natriuretic peptide from the venom of the mammal, *Ornithorhynchus anatinus*, the Australian platypus. *FEBS Lett.* **524**, 172–176 (2002).
30. N. Fujii, T. Takata, N. Fujii, K. Aki, H. Sakaue, D-amino acids in protein: The mirror of life as a molecular index of aging. *Biochim. Biophys. Acta: Proteins Proteom.* **1866**, 840–847 (2018).
31. C. Y. Jing *et al.*, Multiple domestications of Asian rice. *Nat. Plants* **9**, 1221–1235 (2023).
32. A. Gutierrez, T. Yoshimura, Y. Fuchikami, N. Esaki, Modulation of activity and substrate specificity by modifying the backbone length of the distant interdomain loop of D-amino acid aminotransferase. *Eur. J. Org. Chem.* **267**, 7218–7223 (2000).
33. J. Kobayashi, Y. Shimizu, Y. Mutaguchi, K. Doi, T. Ohshima, Characterization of D-amino acid aminotransferase from *Lactobacillus salivarius*. *J. Mol. Catal. B Enzym.* **94**, 15–22 (2013).
34. K. Tanizawa, Y. Masu, S. Asano, H. Tanaka, K. Soda, Thermostable D-amino acid aminotransferase from a thermophilic *Bacillus* species. Purification, characterization, and active site sequence determination. *J. Biol. Chem.* **264**, 2445–2449 (1989).
35. K. Yonaha, H. Misono, T. Yamamoto, K. Soda, D-amino acid aminotransferase of *Bacillus sphaericus*. Enzymologic and spectrometric properties. *J. Biol. Chem.* **250**, 6983–6989 (1975).
36. J. Suarez *et al.*, *AtDAT1* is a key enzyme of D-amino acid stimulated ethylene production in *Arabidopsis thaliana*. *Front. Plant Sci.* **10**, 1609 (2019).
37. T. Yamane, D. L. Miller, J. J. Hopfield, Discrimination between D- and L-tyrosyl transfer ribonucleic acids in peptide chain elongation. *Biochemistry* **20**, 7059–7064 (1981).
38. M. T. Englander *et al.*, The ribosome can discriminate the chirality of amino acids within its peptidyl-transferase center. *Proc. Natl. Acad. Sci. U.S.A.* **112**, 6038–6043 (2015).
39. S. Q. Du, M. Wey, D. Armstrong, D-amino acids in biological systems. *Chirality* **35**, 508–534 (2023).
40. N. Kondori *et al.*, Focus on the role of D-serine and D-amino acid oxidase in amyotrophic lateral sclerosis/motor neuron disease (ALS). *Front. Mol. Biosci.* **5**, 8 (2018), 10.3389/fmolb.2018.00008.
41. H. Yasuda, S. Hirose, T. Kawakatsu, Y. Wakasa, F. Takaiwa, Overexpression of BiP has inhibitory effects on the accumulation of seed storage proteins in endosperm cells of rice. *Plant Cell Physiol.* **50**, 1532–1543 (2009).
42. J. Zhu, B. S. Weir, Analysis of cytoplasmic and maternal effects. II. Genetic models for triploid endosperms. *Theor. Appl. Genet.* **89**, 160–166 (1994).
43. A. Chettoor *et al.*, Maternal gametophyte effects on seed development in maize. *Genetics* **204**, 233–248 (2016).
44. E. T. Wang *et al.*, Control of rice grain-filling and yield by a gene with a potential signature of domestication. *Nat. Genet.* **40**, 1370–1374 (2008).
45. H. Lam *et al.*, D-amino acids govern stationary phase cell wall remodeling in bacteria. *Science* **325**, 1552–1555 (2009).
46. L. Bai *et al.*, Characterization of GdFFD, a D-amino acid-containing neuropeptide that functions as an extrinsic modulator of the *Aplysia* feeding circuit. *J. Biol. Chem.* **288**, 32837–32851 (2013).
47. H. G. Kang, S. Park, M. Matsuoka, G. An, White-core endosperm *floury endosperm-4* in rice is generated by knockout mutations in the C_4-type pyruvate orthophosphate dikinase gene (*OsPPDKB*). *Plant J.* **42**, 901–911 (2005).
48. C. Peng *et al.*, *FLOURY ENDOSPERM6* encodes a CBM48 domain-containing protein involved in compound granule formation and starch synthesis in rice endosperm. *Plant J.* **77**, 917–930 (2014).
49. M. Jin *et al.*, Targeted mutagenesis in rice using CRISPR-Cas system. *Cell Res.* **23**, 1233–1236 (2013).
50. Y. Hiei, T. Komari, *Agrobacterium*-mediated transformation of rice using immature embryos or calli induced from mature seed. *Nat. Protoc.* **3**, 824–834 (2008).
51. S. Chen *et al.*, A highly efficient transient protoplast system for analyzing defence gene expression and protein-protein interactions in rice. *Mol. Plant Pathol.* **7**, 417–427 (2010).
52. Y. Wang *et al.*, GOLGI TRANSPORT 1B (GOT1B) regulates protein export from the endoplasmic reticulum in rice endosperm cells. *Plant Cell* **28**, 2850–2865 (2016).
53. K. J. Livak, T. D. Schmittgen, Analysis of relative gene expression data using real-time quantitative PCR and the $2-\Delta\Delta$CT method. *Methods* **25**, 402–408 (2001).
54. F. Wang *et al.*, ZmTE1 promotes plant height by regulating intercalary meristem formation and internode cell elongation in maize. *Plant Biotechnol. J.* **20**, 526–537 (2022).
55. D. Gordes, U. Kolukisaoglu, K. Thurow, Uptake and conversion of d-amino acids in *Arabidopsis thaliana*. *Amino Acids* **40**, 553–563 (2011).
56. H. Brückner, C. Kellerhoehl, HPLC separation of DL-amino acids derivatized with N^2-(5-Fluoro-2, 4-Dinitrophenyl)-L-amino acid-amides. *Chromatographia* **30**, 621–629 (1990).
57. X. Xu *et al.*, Mass spectrometry-based deep coverage proteome: Evaluation of cellular protein extraction methods. *Chem. J. Chin. Univ.* **45**, 20240344 (2024).
58. X. Xu *et al.*, High-coverage stereoproteome mapping uncovers pervasive protein stereoisomerization associated with neurodegeneration. *Anal. Chem.* **97**, 7814–7824 (2025).
59. H. Dong *et al.*, RNA-seq analysis of developing endosperm at 9 DAF in WT and daat1 rice. NCBI Sequence Read Archive. https://www.ncbi.nlm.nih.gov/bioproject/PRJNA1426511. Deposited 20 February 2026.
60. H. Dong *et al.*, Mass spectrometry-based proteomics of 9 DAF rice seeds. PRIDE, ProteomeXchange. https://www.ebi.ac.uk/pride/archive/projects/PXD059692. Deposited 13 January 2025.